ADVANCED MATERIALS INTERFACES

www.advmatinterfaces.de

Bifunctional Electrocatalysis on Pd-Ni Core–Shell Nanoparticles for Hydrogen Oxidation Reaction in Alkaline Medium

*Meital Shviro, Shlomi Polani, Rafal E. Dunin-Borkowski, and David Zitoun**

The development of alkaline exchange membrane fuel cell (AEMFC) is limited by the sluggish reaction at the anode. Even precious group metals (PGMs) are not effective hydrogen oxidation reaction (HOR) electrocatalysts in alkaline medium. In this manuscript, the original synthesis of effective HOR electrocatalysts for AEMFC is reported. Here, the limitations of using metal-organic precursors are described and their replacement with organometallic precursors is proposed. It is shown that completely different nanostructures can be synthesized by the organometallic route, resulting in the formation of NiPd nano-alloy or Ni@Pd core–shell nanoparticles, instead of Pd@Ni. The presence of both Pd and Ni on the catalyst surface has a drastic effect on its HOR activity, due to a bifunctional electrocatalytic mechanism with hydrogen binding on Pd and OH binding on Ni. The highest activity is measured for NiPd nano-alloy, whose specific activity reaches 104 mA mg_{Pd}^{-1} and 1.38 mA cm_{Pd}^{-2} at 0.1 V versus reversible hydrogen electrode at 298 K. These are the highest values reported so far for an NiPd catalyst. By design, the synthetic approach is generic and can be applied to any pair of metals, either PGM or other transition metals, to synthesize alloyed or core–shell electrocatalysts.

1. Introduction

The hydrogen oxidation reaction (HOR) in alkaline medium has been investigated together with the recent development of alkaline membrane fuel cells, also called anion exchange membrane fuel cells (AEMFCs).[1,2] Under alkaline conditions, the HOR activity of the pure platinum-group metal (PGM) catalysts (Pt, Ir and Pd) is significantly reduced by at least two orders of magnitude compared to the same PGMs under acidic conditions.[3–6]

Dr. M. Shviro, S. Polani, Prof. D. Zitoun
Department of Chemistry
Bar-Ilan Institute for Technology and Advanced Materials (BINA)
Bar-Ilan University
Ramat Gan 5290002, Israel
E-mail: david.zitoun@biu.ac.il
Prof. R. E. Dunin-Borkowski
Ernst Ruska-Centre for Microscopy and Spectroscopy
with Electrons and Peter Grünberg Institute
Forschungszentrum Jülich GmbH
52425 Jülich, Germany

The ORCID identification number(s) for the author(s) of this article can be found under https://doi.org/10.1002/admi.201701666.

DOI: 10.1002/admi.201701666

Recent advances in the understanding of PGM surfaces suggest that an improvement in HOR activity can be achieved by the addition of foreign metal atoms, primarily transition metals, either segregated on the surface of PGMs or in the form of bimetallic alloys.[7,8] In addition, alkaline conditions are much less aggressive for most of the transition metals, allowing the use of non-PGM catalysts alone or in combination with PGMs.[1,9–12] Consequently, the alloying or partial coating of low-cost transition metals with a small amount of PGMs should pave the way for high activity, low cost and durable HOR electrocatalysts for AEMFCs. Palladium has been much less investigated than Pt, even though Pd forms alloys with most of the late transition metals and stands close to Pt in terms of the energy of dissociative adsorption of H_2, as shown in the volcano-type plot of the exchange-current density versus the hydrogen binding energy (HBE).[13,14] The main difference between Pd and Pt lies in the tendency of Pd to absorb as well as adsorb hydrogen, which reduces its turnover and complicates the study of pure Pd.[13]

Bimetallic Pd-Ni HOR catalysts have been predicted to outperform pure PGMs in alkaline conditions, due to the presence of oxophilic Ni species together with hydrogen-binding Pd sites, combining in a bifunctional electrocatalyst. Our recent report of partial coating of Ni thin films with Pd has shown that a relatively low Pd coverage of 17% on Ni results in excellent HOR properties.[15] This approach has been implemented on a high-surface-area electrocatalyst, leading to a high power density of 400 mW cm^{-2} in a Pt-free AEMFC.[16] In that work, the decoration of nanoscale Ni with Pd was achieved by aqueous deposition from Pd(II) complexes. However, the Pd-Ni can be optimized further for better utilization of the Pd atoms. A full comparison of Ni/Pd alloy versus core–shell structures has not yet been reported in the context of HOR in alkaline medium.

Several routes for the synthesis of Pd-Ni bimetallic nanoparticles have been explored. Different synthesis routs can lead to the formation of NiPd alloy, core–shell Pd@Ni or core–shell Ni@Pd nanoparticles, depending on the reaction sequence. One-step reduction of Pd(II) and Ni(II) solution usually leads to alloyed nanoparticles with atomic composition according to the stoichiometry of the reagents.[17,18] More

generally, the core–shell structure can be achieved through two-step reactions. Core–shell Pd@Ni nanoparticles were synthesized from the consecutive reduction of H_2PdCl_4 and nickel acetate by the polyol method.[19] This study shows that Pd nanoparticles catalyze the reduction of Ni(II) and induce the deposition of Ni(0) atoms on the surface of Pd nanoparticles. Core–shell Ni@Pd nanoparticles can be synthesized by using a similar two-step reaction in which the order of the precursors is reversed.[20]

The use of organometallic compounds has several advantages when compared to the use of metal salts and metal-organic precursors. Their low valence results in low-energy activation for the formation of nanoparticles.[21] The organometallic complex bis-(cyclooctadiene) nickel (0), $Ni(COD)_2$, undergoes thermal decomposition at 80 °C to yield Ni(0) films and nanocrystals.[22,23] While the organometallic compounds bis-(dibenzylideneacetone)-palladium(0), $Pd(dba)_2$, and tris-(dibenzylideneacetone)-dipalladium(0), $Pd_2(dba)_3$, have successfully yielded Pd(0) nanoparticles.[24,25] The organometallic synthesis of bimetallic Pd-Ni nanoparticles, synthesized from the same organometallic complexes, resulted in the formation of alloys (used as catalysts for hydrogenation).[26] Syntheses from organometallic compounds can be performed at low temperature[22,27] or in a short reaction time,[23] which can stabilize the formation of kinetically controlled particles with out-of-equilibrium structures, as demonstrated by the formation of non-periodic polyhedral structures[28] and high-temperature phases.[29]

In the present study, we investigate the use of both organometallic and metal-acetylacetonate complexes to achieve one-pot reactions of either alloyed or core–shell nanoparticles, depending on the kinetics of decomposition/reduction of the Pd and Ni precursors. As discussed above, we expect organometallic precursors to decompose rapidly and form nanoparticle cores when they are combined with metal-organic complexes. The resulting nanostructures are tested as HOR electrocatalysts, to search for the most active catalysts in the Pd-Ni system.

2. Results and Discussion

2.1. Kinetic Control of the Radial Distribution of Pd and Ni Atoms in the Nanoparticles

The synthesis of monometallic or multimetallic electrocatalysts usually requires the co-reduction of one or more metal salts, metal-organic complexes or organometallic compounds. A one-pot reaction is usually preferred to a multi-step complex reaction and a large majority of publications report the use of a single class of metal-organic or organometallic complexes. Metal-acetylacetonates are popular, stable and affordable complexes. $Ni(acac)_2$ and $Pd(acac)_2$ display the same oxidation state (II) and differ mainly by the lower redox potential of $Ni(acac)_2$ when compared to that of $Pd(acac)_2$. To demonstrate the difference in reactivity of the two complexes, we heated them in benzyl alcohol, a soft reducing agent, at a moderate temperature of $T = 150$ °C for 12 h in a forming gas atmosphere with the addition of polyvinylpyrrolidone as a stabilizing agent. Under these conditions, only $Pd(acac)_2$ reacted while $Ni(acac)_2$ did not.[30]

In contrast, the organometallic complexes $Ni(COD)_2$ and $Pd(dba)_2$ have been commonly used as organometallic precursors for the synthesis of metallic nanoparticles. The kinetics of decomposition slightly favors the formation of Pd. However, to the best of our knowledge the use of both organometallic and metal-organic complexes has not been attempted in a one-pot reaction and is expected to result in the formation of kinetically controlled core–shell nanoparticles, as shown in **Scheme 1**.

The metal-organic precursors yield nanoparticles analyzed by powder X-ray diffraction (PXRD) shown as a blue line in **Figure 1**. The PXRD results reveal the presence of two crystalline phases with lattice constants that are close to those of FCC Ni (JCPDS # 04-0850; Fm-3m, $a = 3.5238$ Å: red lines) and FCC Pd (JCPDS # 05-0681; Fm-3m, $a = 3.8902$ Å: blue lines). The diffractogram can be analyzed as a two-phase material: one Pd-rich and one Ni-rich phase. The peaks are broad due to the small particle size and a more quantitative analysis is not appropriate. No other phases (oxides, hydroxides, or ordered compounds) are observed by PXRD. The organometallic approach yields a very disordered phase with very broad and asymmetric peaks which could match several nano-phases of Ni rich and Pd rich alloys (Figure 1, black line). The mixed approach (organometallic for the Ni and metal-organic for the Pd) yields a more crystalline material with two phases almost matching the lattice constant of the pure Ni and Pd phases.

The nanoparticles were analyzed using transmission electron microscopy (TEM) in high-angle annular dark-field scanning TEM (HAADF-STEM) mode and energy dispersive X-ray spectroscopy (EDX) analysis (**Figure 2**). The nanoparticles display a mean size of 11.3 ± 2 nm with quasi-spherical shape (Figure 2A,B). Pd-Ni atomic ratios inside the particles obtained from EDX line scans (Figure 2D,E) and maps (Figure 2F) for a statistical number of particles. Analysis of the results revealed a gradient in Ni concentration, with the Ni content increasing from the center to the shell of each nanoparticle (Figure 2E). Although EDX analysis has limitations in terms of spatial resolution; within these limitations, the data support the formation of core–shell structures with Pd-rich cores and Ni-rich shells. The nanoparticles are inferred to be core–shell Pd@Ni particles based on their sizes (measured from TEM images), atomic ratios between Pd and Ni (obtained from EDX results from ensembles of nanoparticles) and their atomic distribution (obtained from EDX line scans). The statistical analysis of EDX data gives a Pd/Ni ratio of 1:2 at the centers of the nanoparticles and 1:6 near the surface.

Metal acetylacetonate precursors yielded core–shell Pd@Ni nanoparticles, as expected from the high reactivity of $Pd(acac)_2$ compared to $Ni(acac)_2$ toward reduction in forming gas. Fortunately, the Pd nanoparticles can catalyze the $Ni(acac)_2$ reduction process, leading to the formation of a Ni shell around the Pd core. However, the synthetic pathway falls short of providing a Pd-rich shell of interest for electrocatalysis. Our results differ from previously reported one-pot solvothermal reaction of $Pd(acac)_2$ and $Ni(acac)_2$ in high boiling-point coordination solvents, for which Pd-enriched shell bimetallic nanoparticles were reported.[31]

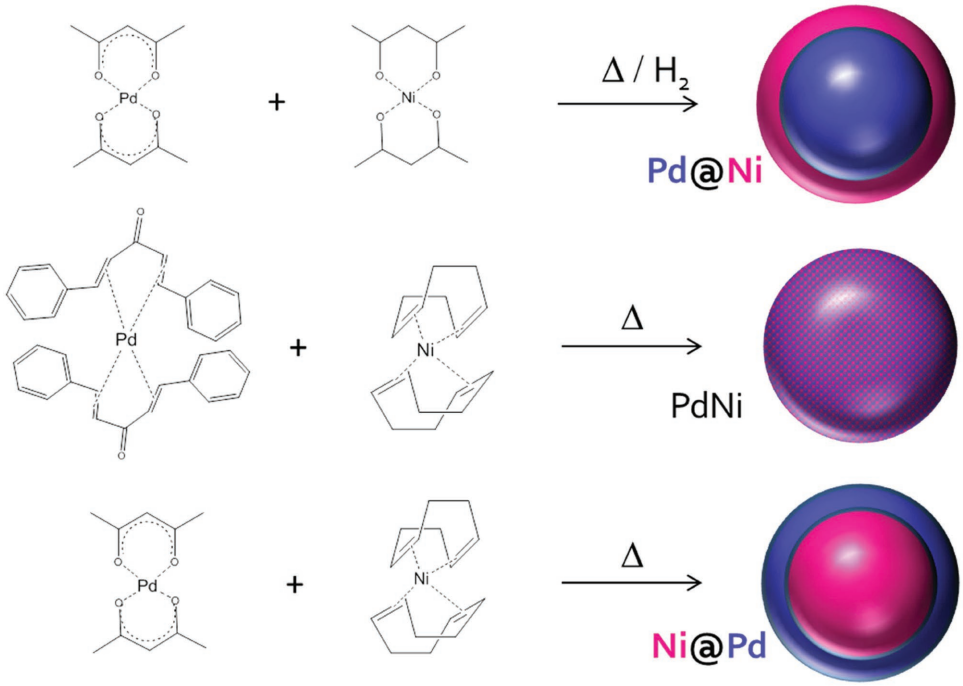

Scheme 1. Metal-organic and organometallic precursors of Pd/Ni bimetallic nanoparticles and corresponding expected radial composition of the nanoparticles.

To confirm this paradigm, the synthesis was performed under comparable conditions of temperature and solvent with zerovalent organometallic precursors $Ni(COD)_2$ and $Pd(dba)_2$ (Scheme 1). The organometallic precursors thermally decompose without need for reducing agents and yield metallic nanoparticles and cyclooctadiene or dibenzylidene acetone by-products. The resulting nanocrystals have been analyzed by TEM, high-resolution HAADF-STEM and EDX elemental mapping (**Figure 3**). The particles were found to have spherical morphology with a mean size of 80 ± 15 nm (Figure 3A). These "secondary" particles present an internal nanotexture with a "primary" particle size of 5 ± 2 nm (Figure 3B). Each primary particle is monocrystalline.

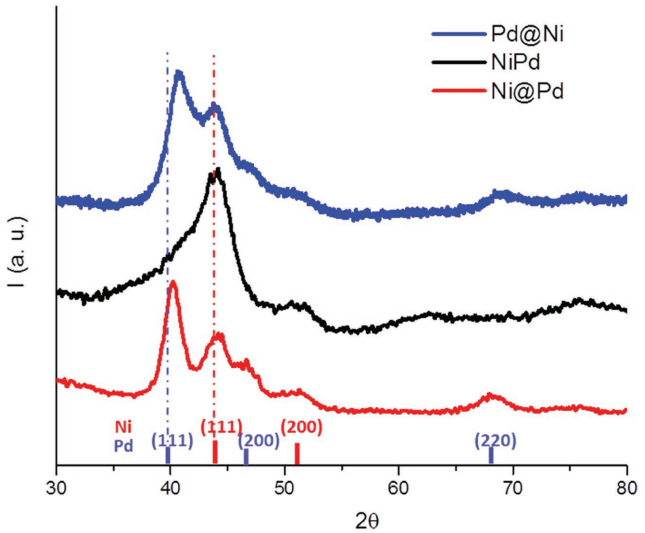

Figure 1. Powder X-ray diffraction (PXRD) patterns of the Ni-Pd samples synthesized following Scheme 1. Pd and Ni reflections are marked by solid lines, with (111) reflections marked by dashed lines.

The atomic distribution of NiPd was assessed by EDX (Figure 3C) and, on the scale of a secondary particle, the stoichiometry was found to be $PdNi_2$. The secondary particles are mapped using EDX, revealing a distribution of Pd and Ni within each particle. On the level of a single particle, EDX correlates with a mixing of Pd and Ni down to nanoscale. It is not clear if a single alloy is formed and the differences in atomic compositions between several areas below the nanoscale may point at the presence of Ni rich and Pd rich regions randomly distributed within the particles. The use of organometallic precursors was found to be successful for achieving a nanoscale mixing of Pd and Ni, while metal acetylacetonates yield a Pd@Ni structure. The atomic distribution correlates with the kinetics of the reaction of the metallic precursors. Organometallic precursors decompose very quickly, yielding many bimetallic nucleation centers ("primary" particles), which further coalesce into secondary particles.

The difference in kinetics was further investigated by using an organometallic precursor of $Ni(COD)_2$ to form the core of the particle and the $Pd(acac)_2$ complex to form the particle shell. The one-pot reaction was conducted under the same conditions as the reaction from the organometallic precursors, and it yielded larger nanocrystals with sizes of 23 ± 4 nm (**Figure 4**A,B). The larger particle size is consistent with the rapid formation of nucleation centers and the slow growth process. The atomic distribution was assessed from EDX line scans (Figure 4D) and elemental maps (Figure 4C). These results confirm the hypothesis that the atomic distribution of metal atoms

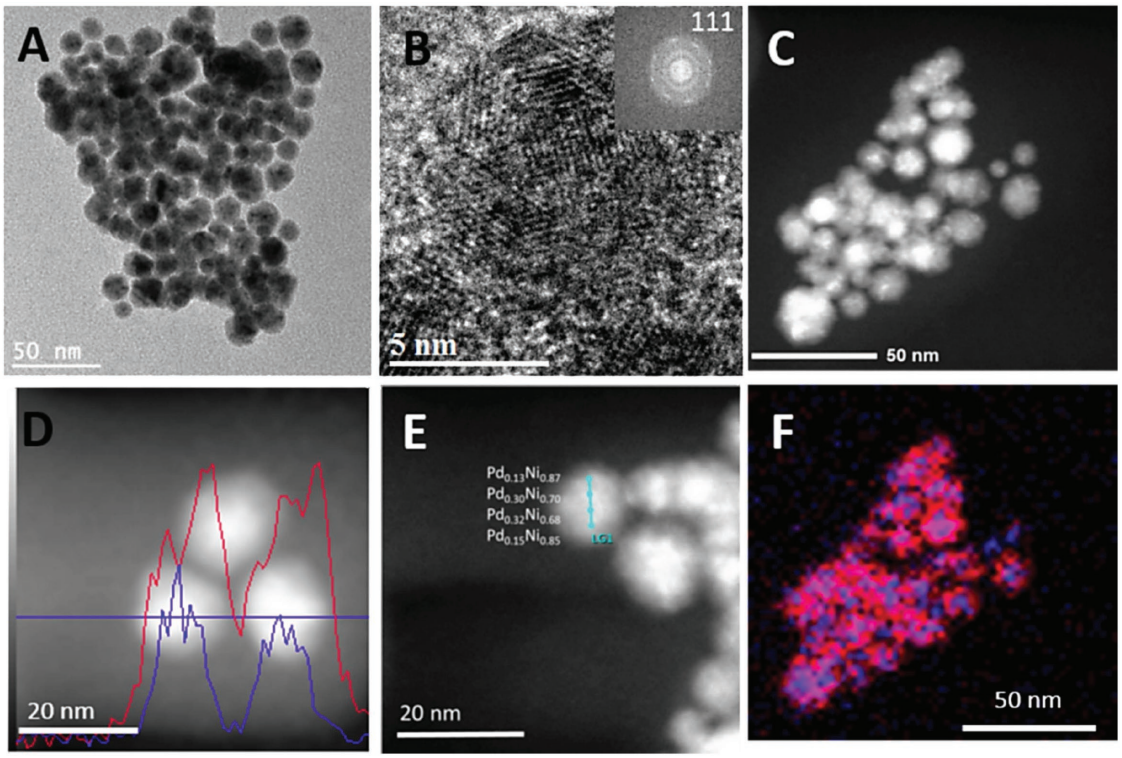

Figure 2. Transmission electron microscopy (TEM) of the Pd@Ni sample: A) Bright-field TEM image of an ensemble of nanoparticles; B) high-resolution TEM image with a fast-Fourier transform; C) high-angle annular dark-field scanning TEM image and F) corresponding composition map recording using electron energy dispersive X-ray spectroscopy (EDX) composition map (Pd: blue and Ni: red); D) EDX line scans for Pd (blue line) and Ni (red line); E) Pd/Ni atomic ratios on measured in a single nanocrystal.

in each nanoparticle can be controlled by the kinetics of decomposition. The fast decomposition rate of the $Ni(COD)_2$ organometallic precursor yields Ni nanoparticles that act as nucleation centers for the further growth of Pd shell. The shell growth may arise from several mechanisms involving the catalytic reduction of $Pd(acac)_2$ on the freshly formed Ni surfaces or the nucleation site preferred by these nuclei. The Pd shell effectively covers all the Ni surface and is found to be a few nm thin (Figure 4C,D). The Ni@Pd nanoparticles form a very interesting model catalyst that we tested together with the Pd@Ni and NiPd alloyed nanoparticles for HOR in alkaline medium.

2.2. Electrochemical Activity of NiPd, Pd@Ni, and Ni@Pd Nanoparticles as HOR Electrocatalysts

Pd-Ni electrocatalyst have been the focus of interest for the investigation of HOR.[15,16] Following the syntheses reported above, a variation of the metallic precursors has been instrumental in the control of the radial atomic distribution of Ni and Pd. Below, we shall refer to the catalysts as NiPd: an alloy from the organometallic synthesis, Pd@Ni: a core–shell from the acetylacetonate precursors and Ni@Pd: a core–shell from the mixed precursor synthesis.

The electrocatalytic activity has been tested under alkaline conditions (0.1 mol L^{-1} KOH) where Ni could sustain thanks to its passivation with $Ni(OH)_2$ while Pd could be reversibly oxidized in the potential window. Considerable effort was devoted to achieving the best experimental conditions and avoiding any contamination from Pt and other metals. The electrochemical cell was glass-free with a working rotating glassy carbon electrode, a glassy carbon counter-electrode and a reversible hydrogen electrode (RHE). A very thin layer (only 5 μg) of the catalyst was spread on the glassy carbon electrode together with a Vulcan XC72 carbon and Nafion polyelectrolyte. Cyclic voltammetry was recorded under Ar after prolonged deoxygenation and stabilization. The potential was scanned between 0.05 and 1.35 V and normalized to the geometrical surface (0.196 cm^2) of the glassy carbon.

Commercial Pd black (7 ± 3 nm) was measured as reference for HOR activity (**Figure 5**). The electrochemical surface area (ECSA) was measured from the cathodic peak at 0.65 V/RHE, which is related to the reduction of oxygen species on Pd.

In contrast, the Pd@Ni sample shows a "flat" cyclic voltammetry without any activity toward hydrogen adsorption/desorption (Figure 5A). These results are consistent with a surface fully covered with $Ni(OH)_2$ and "free" of active Pd sites. The NiPd catalyst shows a much more interesting cyclic voltammetry with a cathodic peak at 0.55 V/RHE (Figure 5A). This peak arises from the reduction of oxygen species on a metallic surface. In fact, the potential slightly differs from the reduction of oxygen species on pure Pd surfaces (0.65 V/RHE), hinting at the alloyed nature of the surface. The region of underpotential desorption (UPD) hydrogen shows the sorption/desorption on the catalyst but is not defined enough to show clear data on the ECSA and on the specific binding sites. Ni@Pd samples

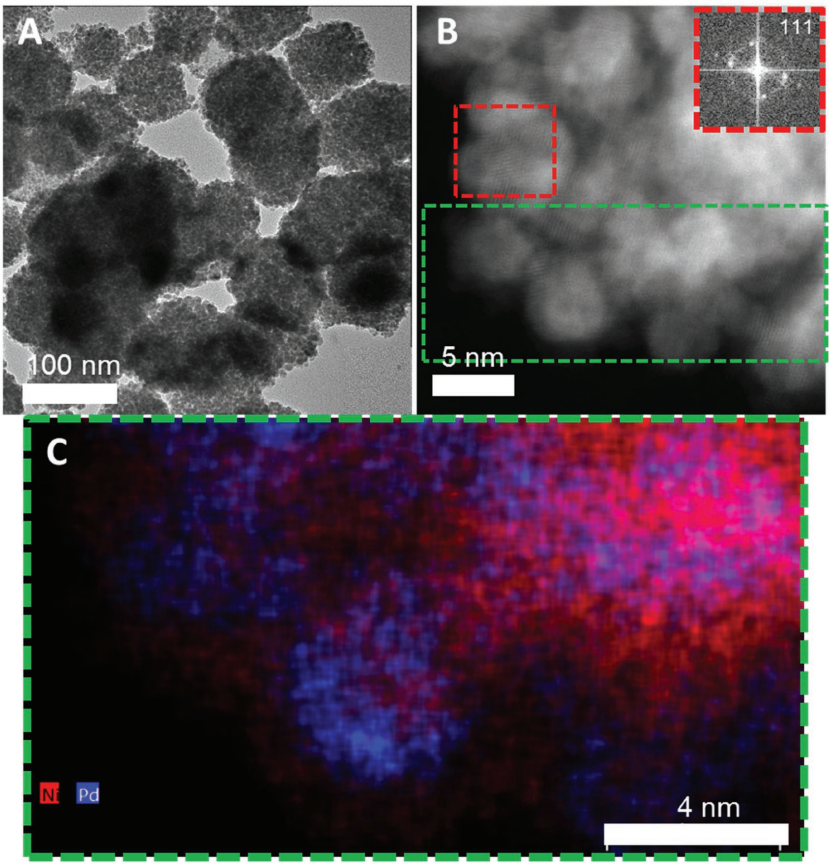

Figure 3. TEM of NiPd sample: A) TEM image of ensemble of nanoparticles; B) HAADF-STEM image with an FFT of the area in the red square inset; C) EDX composition map of the green area in (B) (Pd: blue and Ni: red).

show a cyclic voltammetry typical of Pd with a cathodic peak at 0.65 V/RHE and a well-defined UPD region.

The HOR activity was recorded on the rotating disc electrode at 900 rpm in an H_2-saturated solution at $T = 298$ K. The J–V curves were recorded from open circuit voltage (OCV) up to 1 V and backward. The negatively scanned curves are shown in Figure 5B to discard the hydrogen absorption in Pd. Pure Pd nanopowder shows very sluggish activity with a high onset potential and reaches the half-wave potential at 0.47 V which impedes its use as an anode catalyst in fuel cells. For the bimetallic samples, the HOR shows very different behavior and, as expected, no activity at all for the Pd@Ni sample. This result is a striking proof that the surfaces of these nanoparticles are completely passivated by $Ni(OH)_2$ even with a Pd core below the Ni shell.

Moreover, NiPd and Ni@Pd are highly active as HOR electrocatalysts. The onset potential is very low, almost comparable to a Pt catalyst and close to 0 V/RHE. The current density of the geometrical surface of Ni@Pd is comparable to that of the NiPd sample even if the alloyed sample reaches the plateau a lower potential. At 0.1 V versus RHE, the current density per geometrical surface area reaches 0.37 mA cm^{-2} for Ni@Pd compared to 0.52 mA cm^{-2} for the NiPd catalyst.

The ECSA can be deduced from the calculation of the Pd-active surface area using several approximations. The most accurate method involves the surface area attributed to the UPD of hydrogen, as seen in the cyclic voltammetry (**Figure 6**). In the case of nanoparticles under alkaline conditions, the approximation is very crude since the region is not very well defined. The second method involves approximating the reduction of the Pd oxygen species as a surface-only process which is specific to Pd surface atoms (Figure 5A). The ECSA was also calculated by CO stripping experiment at 200 mV s^{-1} where the active sites toward hydrogen are approximated with the coordination sites of chemisorbed CO molecules (Figure 6A). Qualitatively, the CO stripping gives a straightforward way to distinguish between metallic surfaces (Ni@Pd and NiPd) and hydroxide passivated ones (Pd@Ni) (Figure 6A). The onset potential for the CO oxidation also increases from the Ni@Pd toward the NiPd alloyed nanoparticles. The spectrum is complex and reveals different binding sites for the CO on the metallic surfaces. Whether the different peaks correspond to different crystallographic planes, defects or chemical nature is still a matter of debate even for flat surfaces.[32] Therefore, the calculations of the ECSA should be regarded cautiously, and they provide only an estimate of the active surface of the catalysts (Figure 6B). The ECSA values obtained from the reduction in Pd oxygen species and CO stripping are overall consistent.

Normalized values of the current density per Pd surface area show that the activity of the NiPd alloyed surface is higher than that of the pure Pd and Ni@Pd electrocatalysts (**Figure 7**A). Pd and Ni@Pd display comparable surface activity which is consistent with the monometallic "Pd" nature of the surfaces. The specific activity of the NiPd alloy 1.38 mA cm^{-2}_{Pd} is 7 times higher than that of Pd, which points at the role of Ni as a catalyst or a co-catalyst for HOR.

The better utilization of Pd in Ni@Pd versus Pd is well reflected by its mass activity, which is 10 times higher for the core–shell Ni@Pd (Figure 7B) and 13 times higher than Pd under the same conditions (0.1 V vs RHE). This striking result shows the benefits of alloying the surface with Ni under alkaline conditions, as already demonstrated for oxygen reduction reaction alloyed catalysts.[33]

2.3. General Rules for the Design of Electrocatalysts

In terms of the synthetic approach developed here, the results provide general rules for the design of surface PGM-enriched electrocatalysts. Core–shell catalysts with PGM shells have attracted wide interest, in order to minimize the cost of PGMs on electrocatalysts. Core–shell structures have been achieved by using sequential reactions and spontaneous segregation from a single-pot reaction. However, this reaction is specific to only a

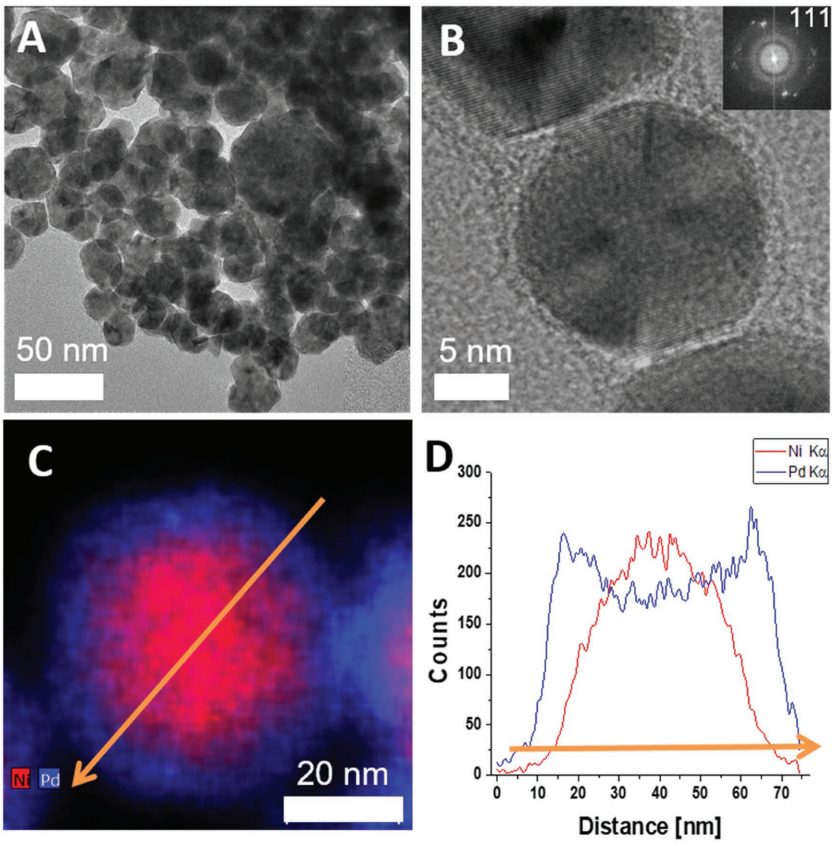

Figure 4. TEM of Ni@Pd sample: A) TEM image of ensemble of nanoparticles;(B) HRTEM image with FFT inset; C) EDX composition map (Pd: blue and Ni: red); D) EDX line scans showing Pd (blue) and Ni (red).

few metals. In our approach, the core–shell structure is directed by the kinetics of decomposition of the precursors. Roughly speaking, any core–shell geometry can be achieved by starting with reactive precursors (typically, organometallic compounds) for the core and less reactive precursors (typically, metal organic complexes) for the shell in a versatile scheme.

A relationship between the atomic distribution and the high HOR activity of NiPd bimetallic nanoparticles has been demonstrated in the present study. The most popular acetylacetonates metal-organic precursors lead to a Pd@Ni structure which is clearly not a good catalyst. An organometallic Ni(0) with faster decomposition kinetics leads to an enrichment of the shell with Pd, either in the form of Ni@Pd with a Pd(II) metal-organic complex or as a nanoscale alloy with a Pd(0) organometallic precursor. The latter alloyed structure shows by far the best activity per Pd atom on the surface, which suggests the importance of Ni species on the surface and not only in the core of the nanoparticle. Below, we discuss the origin of such a synergistic effect between Ni and Pd.

The origin of the low HOR catalytic activity of Pd in alkaline environments still needs the agreement of the scientific community. Since hydrogen atom desorption is widely viewed as a rate-determining step, the role of Ni foreign atoms on the surface which facilitate this process has been interpreted as a "bifunctional" activity. As mentioned in the introduction, examples have been given for the beneficial effects of alloying on HOR rate enhancement in alkaline media, which is due to either electronic effects modifying the HBE or added oxophilicity. Referring now to the possibility that the effect of a second component in such HOR binary metal catalysts is only electronic, resulting in a weakening of the M—H bond at the surface of a first component, we note that this argument was made in the context of Ru added to Pt[34] and of Mo and Co added to Ni[9] to generate binary or ternary alloys. However, in our previous studies of Ni surfaces covered with Pd, the decrease of activity per Pd atom with increase coverage clearly demonstrates the prominent role of the oxophilicity, i.e., the high hydroxide local concentrations near the Ni species to promote the $H_{ab} + OH^- \rightarrow H_2O + e^- + *$ Volmer step of the HOR reaction. In the case of NiPd alloyed nanoparticles synthesized here, the surface is rich both in Pd and Ni site, which provide an excellent case for adsorbing pairs of H and OH groups. This hypothesis supports the high activity of 104 mA mg_{Pd}^{-1} and 1.38 mA cm_{Pd}^{-2} at 0.1 V versus RHE at 298 K obtained for the NiPd alloy.

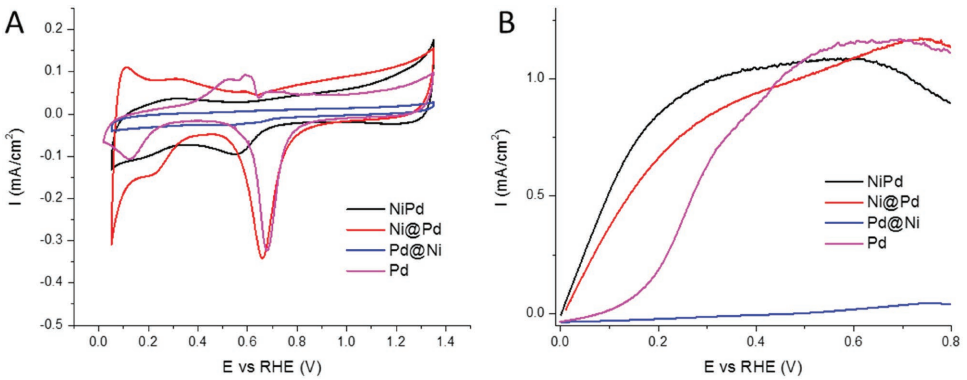

Figure 5. A) Cyclic voltammograms recorded at 298 K in an Ar-saturated solution at 50 mV s^{-1}; B) Ohmic loss-corrected polarization curves recorded in a H_2-saturated atmosphere at 5 mV s^{-1} and 900 rpm (the negative scanning direction is shown).

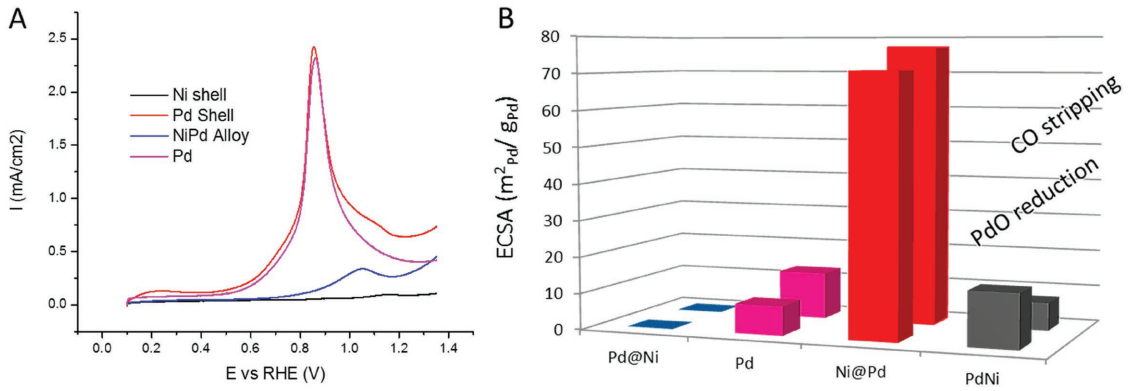

Figure 6. A) CO stripping at 200 mV s^{-1} starting from E_{ads} = 0.1 V; B) ECSA obtained from PdO cathodic reduction and CO stripping.

3. Conclusions

We have demonstrated the limitations of classical metal-organic $Ni(acac)_2$ and $Pd(acac)_2$ complexes as precursors for HOR electrocatalysts. They yield Ni surface-rich electrocatalyst Pd@Ni, with sluggish HOR properties. In contrast, the organometallic precursors $Ni(COD)_2$ and $Pd(dba)_2$ yield NiPd nanoalloys. A mixed approach, involving the use of $Ni(COD)_2$ and $Pd(acac)_2$, allows for the synthesis of Ni@Pd core–shell nanoparticles. The radial distributions of Ni and Pd in the nanoparticles are found to be guided by the kinetics of the reactions of the precursors, with a much faster reaction of the organometallic species yielding the nanocrystal cores. The distribution of the two metals within the nanocrystals has a large influence on the electrocatalytic activity of the Pd-Ni nanoparticles that we tested for HOR in alkaline medium. The highest activity was measured for NiPd alloyed nanoparticles synthesized by the organometallic route with the resulting specific activity reaching 104 mA mg^{-1}_{Pd} and 1.38 mA cm^{-2}_{Pd} at 0.1 V versus RHE. These alloyed nanoparticles have a mass activity that is 13 times higher than pure Pd nanoparticles, due to a synergistic electrocatalytic effect between the Ni and Pd surface atoms. By design, the synthetic approach is generic and can be applied to any pair of metals, either PGM or other transition metals, to synthesize alloyed or core–shell electrocatalysts.

4. Experimental Section

Materials: Benzylalcohol (99%, pure) and (99+%, anhydrous <50 ppm) was acquired from ACROS. Benzoic acid (ACS, 99.5%) and poly(vinylpyrrolidone) (PVP), (MW = 8000, AR) were purchased from Alfa Aesar. Palladium (II) acetylacetonate ($Pd(acac)_2$) (STREM, 98%), $Ni(COD)_2$ (STREM, 98%), $Pd(dba)_2$ (STREM, 98%), Nickel (II) acetylacetonate ($Ni(acac)_2$), (95%, Sigma Aldrich) were used without further purification. Pd nanopowder (QuantumSphere) was used as received.

Synthesis of Pd@Ni Nanocrystals (Metal-Organic Precursors): In a typical synthesis of Pd@Ni nanocrystals, $Pd(acac)_2$, (0.2 mmol), poly(vinylpyrrolidone) (PVP, MW = 8000), (0.08 g) $Ni(acac)_2$ (0.93 mmol) and benzoic acid (4.0 mmol) were dissolved in 50 mL of benzyl alcohol by vigorous stirring for 30 min. The resulting homogeneous green solution was transferred into a 100 mL Ace pressure glass flask. The sealed vessel was then heated to 150 °C for 12 h and was then cooled down to room temperature. The products were precipitated by acetone, separated via centrifugation, and further purified by an ethanol/acetone mixture.

Synthesis of NiPd Alloyed Nanocrystals (Organometallic Precursors): $Ni(COD)_2$ (0.39 mmol) and $Pd(dba)_2$ (1.02 mmol) were dissolved in 3 mL of anhydrous benzyl alcohol in a glovebox. The solution was then transferred to a special sealed vial for microwave reaction (CEM Discover) and heated at 170 °C (run time 2 min, hold time from 5 min). The products were separated via centrifugation, and further purified by an ethanol/toluene mixture.

Synthesis of Ni@Pd Nanocrystals (Organometallic/Metal-Organic Precursors): $Ni(COD)_2$ (0.39 mmol) and $Pd(acac)_2$ (1.74 mmol) were dissolved in 3 mL of anhydrous benzyl alcohol in a glovebox. The

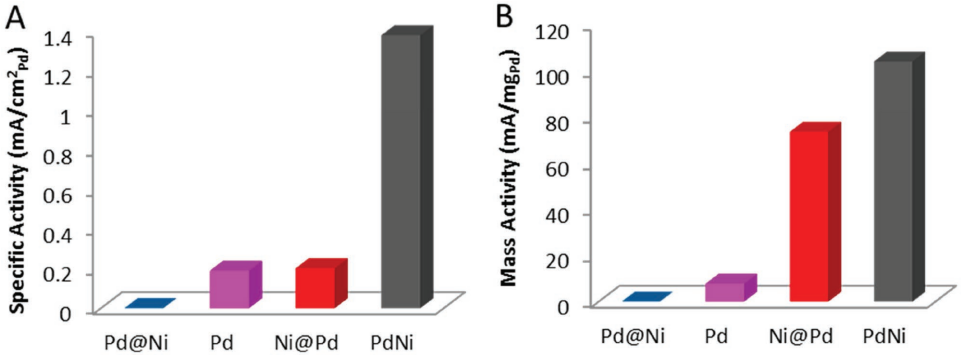

Figure 7. A) Specific activity and B) Pd mass activity of the electrocatalysts measured from the RDE experiment (900 rpm, 0.1 V vs RHE, T = 298 K, i-R corrected).

solution was then transferred to a special sealed vial for microwave reaction (CEM Discover) and heated at 170 °C (run time 2 min, hold time from 5 min). The products were separated via centrifugation, and further purified by an ethanol/toluene mixture.

Structural Characterization: HRTEM study was carried out at 200 kV on a JEOL JEM-2100 (LaB6) TEM. Fast Fourier transform (FFT) analysis of HRTEM images was used for structural analysis. HRTEM images and EDX measurements were obtained at 200 kV on a JEOL JEM-2100F TEM. Scanning TEM (STEM) was performed at 200 kV on an FEI Titan 80–200 ("ChemiSTEM") TEM,[35] equipped with a C_S probe corrector (CEOS GmbH) and a high-angle annular dark field (HAADF) detector operated at 200 kV. In order to achieve "Z-Contrast" conditions a probe semi-angle of 25 mrad and an inner detector collection semi-angle of the detector of 88 mrad were used. EDX Compositional maps were obtained using four symmetric large-solid-angle silicon drift detectors. For EDX measurement an FEI double-tilt holder was used and the TEM specimen was untilted. EDX analysis was performed using ESPRIT software (Bruker Company, Berlin, Germany) using the Ni K and Pd L peaks. The crystalline phases and crystallinity of the prepared powders of the final products were determined using XRD with Cu Ka (0.1541 nm) radiation (Rigaku SmartLab).

Electrochemical Measurements: Electrochemical measurements were performed in a polypropylene cell in a three-electrode configuration using a polished 0.196 cm^2 glassy carbon disk as working electrode, a glassy carbon rod as a counter electrode and RHE as a reference electrode. The catalyst loading on the glassy electrode was 5 µg. The alkaline solution was prepared from KOH (Sigma-Aldrich, 99.998%) and ultrapure water. The glassy carbon was mounted on a rotating electrode (Pine instruments) and all data were collected using a VMP3 potentiostat (Bio-Logic) impedance channel. Potentials were corrected for ohmic losses, measured by impedance spectroscopy before each polarization curve. All of the gases that were used were of the highest purity available (99.999%). After purging in Ar for 15 min, the voltammograms were collected at 50 mV s^{-1} after stabilization for 50 cycles from 0.05 to 1.35 V versus RHE. Polarization curves were recorded after saturation of the solutions with H_2 by sweeping from OCV to 1 V versus RHE (positive going scan) and back (negative going scan) at 5 mV s^{-1} using different rotating speeds (225, 400, 625, 900, 1600 rpm) (only the 900 rpm results are shown). CO stripping was performed at 5, 10, 20, 50, 100, 200, and 500 mV s^{-1} after CO saturation of the catalysts (only the 200 mV s^{-1} results are shown).

Acknowledgements

This work was partially supported the TEPS Magnet program, Office of the Chief Scientist (OCS), Ministry of Economy and Industry, Israel and by the Planning & Budgeting Committee of the Council of High Education and the Prime Minister Office of Israel, in the framework of the INREP project (Israel National Research Center on Electrochemical Propulsion). The authors acknowledge Dr. Marc Heggen for fruitful discussions and his constant support for the project.

Conflict of Interest

The authors declare no conflict of interest.

Keywords

alkaline fuel cells, electrocatalysis, hydrogen oxidation reaction, nickel, organometallic

Received: December 21, 2017
Revised: January 18, 2018
Published online:

[1] S. Lu, J. Pan, A. Huang, L. Zhuang, J. Lu, *Proc. Natl. Acad. Sci. USA* **2008**, *105*, 20611.
[2] J. R. Varcoe, P. Atanassov, D. R. Dekel, A. M. Herring, M. a. Hickner, P. a. Kohl, A. R. Kucernak, W. E. Mustain, K. Nijmeijer, K. Scott, T. Xu, L. Zhuang, *Energy Environ. Sci.* **2014**, *7*, 3135.
[3] N. M. Markovic, H. A. Gasteiger, P. N. Ross, *J. Phys. Chem.* **1996**, *100*, 6715.
[4] W. Sheng, H. a. Gasteiger, Y. Shao-Horn, *J. Electrochem. Soc.* **2010**, *157*, B1529.
[5] P. Rheinlander, S. Henning, J. Herranz, H. A. Gasteiger, *ECS Trans.* **2012**, *50*, 2163.
[6] J. Durst, A. Siebel, C. Simon, F. Hasche, J. Herranz, H. a. Gasteiger, *Energy Environ. Sci.* **2014**, *7*, 2255.
[7] R. Subbaraman, N. Danilovic, P. P. Lopes, D. Tripkovic, D. Strmcnik, V. R. Stamenkovic, N. M. Markovic, *J. Phys. Chem. C* **2012**, *116*, 22231.
[8] R. Subbaraman, D. Tripkovic, D. Strmcnik, K.-C. Chang, M. Uchimura, A. P. Paulikas, V. Stamenkovic, N. M. Markovic, *Science* **2011**, *334*, 1256.
[9] W. Sheng, A. P. Bivens, M. Myint, Z. Zhuang, R. V. Forest, Q. Fang, J. G. Chen, Y. Yan, *Energy Environ. Sci.* **2014**, *7*, 1719.
[10] A. Manzo-Robledo, N. J. S. Costa, K. Philippot, L. M. Rossi, E. Ramírez-Meneses, L. P. A. Guerrero-Ortega, S. Ezquerra-Quiroga, *J. Nanoparticle Res.* **2015**, *17*, 1.
[11] T. Mikolajczyk, M. Turemko, B. Pierozynski, *J. Electroanal. Chem.* **2014**, *735*, 32.
[12] A. Zadick, L. Dubau, K. Artyushkova, A. Serov, P. Atanassov, M. Chatenet, *Nano Energy* **2017**, *37*, 248.
[13] M. Shao, *J. Power Sources* **2011**, *196*, 2433.
[14] W. Sheng, M. Myint, J. G. Chen, Y. Yan, *Energy Environ. Sci.* **2013**, *6*, 1509.
[15] I. Bakos, A. Paszternák, D. Zitoun, *Electrochim. Acta* **2015**, *176*, 1074.
[16] M. Alesker, M. Page, M. Shviro, Y. Paska, G. Gershinsky, D. R. Dekel, D. Zitoun, *J. Power Sources* **2016**, *304*, 332.
[17] D. J. Ham, C. Pak, G. H. Bae, S. Han, K. Kwon, S.-A. Jin, H. Chang, S. H. Choi, J. S. Lee, *Chem. Commun.* **2011**, *47*, 5792.
[18] F. Miao, B. Tao, P. K. Chu, *Dalton Trans.* **2012**, *41*, 5055.
[19] T. Teranishi, M. Miyake, *Chem. Mater.* **1999**, *11*, 3414.
[20] K. Nagaveni, A. Gayen, G. N. Subbanna, M. S. Hegde, *J. Mater. Chem.* **2002**, *12*, 3147.
[21] H. Bonnemann, G. Khelashvili, *Appl. Organomet. Chem.* **2010**, *24*, 257.
[22] M. Shviro, D. Zitoun, *Nanoscale* **2012**, *4*, 762.
[23] M. Shviro, D. Zitoun, *RSC Adv.* **2013**, *3*, 1380.
[24] A. Duteil, R. Quéau, B. Chaudret, R. Mazel, C. Roucau, J. S. Bradley, *Chem. Mater.* **1993**, *5*, 341.
[25] M. Guerrero, N. J. S. Costa, L. L. R. Vono, L. M. Rossi, E. V. Gusevskaya, K. Philippot, *J. Mater. Chem. A* **2013**, *1*, 1441.
[26] N. J. S. Costa, M. Guerrero, V. Collie, E. Teixeira-neto, R. Landers, K. Philippot, L. M. Rossi, *ACS Catal.* **2014**, *4*, 1735.
[27] M. Shviro, A. Paszternák, A. Chelly, D. Zitoun, *J. Nanoparticle Res.* **2013**, *15*, 1823.
[28] A. Rodriguez, C. Amiens, B. Chaudret, M.-J. Casanove, P. Lecante, J. S. Bradley, *Chem. Mater.* **1996**, *8*, 1978.
[29] N. Cordente, M. Respaud, F. Senocq, M.-J. Casanove, C. Amiens, B. Chaudret, *Nano Lett.* **2001**, *1*, 565.
[30] Y. Wu, S. Cai, D. Wang, W. He, Y. Li, *J. Am. Chem. Soc* **2012**, *134*, 8975.
[31] S. U. Son, Y. Jang, J. Park, H. Bin Na, H. M. Park, H. J. Yun, J. Lee, T. Hyeon, *J. Am. Chem. Soc.* **2004**, *126*, 5026.
[32] G. García, M. T. M. Koper, *Phys. Chem. Chem. Phys.* **2009**, *11*, 11437.
[33] V. Mazumder, M. Chi, K. L. More, S. Sun, *J. Am. Chem. Soc.* **2010**, *132*, 7848.
[34] Y. Wang, G. Wang, G. Li, B. Huang, J. Pan, Q. Liu, J. Han, L. Xiao, J. Lu, L. Zhuang, *Energy Environ. Sci.* **2015**, *8*, 177.
[35] A. Kovács, R. Schierholz, K. Tillmann, *J. Large Scale Res. Facil.* **2016**, *2*, A43.